Operation and control of a Current Source Converter series tapping of an LCC-HVDC link for integration of Offshore Wind Power Plants

Joan Sau-Bassols[a], Eduardo Prieto-Araujo[a], Samuel Galceran-Arellano[a], Oriol Gomis-Bellmunt[a,b]

[a] *Centre d'Innovació Tecnològica en Convertidors Estàtics i Accionaments (CITCEA-UPC), Departament d'Enginyeria Elèctrica, Universitat Politècnica de Catalunya. ETS d'Enginyeria Industrial de Barcelona, Av. Diagonal, 647, Pl. 2. 08028 Barcelona, Spain (joan.sau@citcea.upc.edu)*
[b] *IREC Catalonia Institute for Energy Research, Barcelona, Spain*

Abstract

This work presents a series tapping station for integrating Offshore Wind Power Plants (OWPP) into a (Line Commutated Converter High Voltage Direct Current) LCC-HVDC transmission system. The tapping station allows to integrate wind power resources without building a new HVDC link and it is based on a Current Source Converter (CSC). However, the CSC requires a minimum DC current to extract the power coming from the OWPP which may not be guaranteed depending on the power conditions of the HVDC corridor. For this reason, this paper proposes a coordinated operation and control of the CSC and the OWPP. A steady-state analysis is performed to determine the appropriate AC voltage level of the CSC. A power reduction algorithm is presented to limit power extraction during a reduction in the current of the HVDC transmission system and under loss of communications between the CSC and the OWPP. The proposed algorithm and the performance of the system are validated through simulation results

Keywords: HVDC transmission, LCC-HVDC, Current-Source Converter (CSC), Offshore Wind Power Plant, Tapping station.

Email address: joan.sau@citcea.upc.edu . Tel. +34 934054246 Fax. +34 934017433 (Joan Sau-Bassols)

1. Introduction

Currently, offshore wind energy appears to be a promising renewable source and it is expected that the installed capacity in Europe will reach 66 GW by the end of 2030 [1]. The traditional HVAC transmission suffers from important drawbacks when Offshore Wind Power Plants (OWPP) are located far from the coast. Then, the preferred technology is High Voltage Direct Current (HVDC) since it offers lower losses when long distances and undersea cables are considered [2], [3].

Traditionally, HVDC technology employs Line Commutated Converters (LCCs) based on thyristors [4]. LCC-HVDC is a mature and reliable technology with many stations interconnecting mainland and islands, using point-to-point connections. Fig. 1 shows the existing LCC-HVDC transmission links using undersea cables in the Northern Europe [5]. These links can be located near to potential OWPP. However, one important drawback of HVDC is the difficulty of supplying or injecting reduced amount of power in the vicinity of the HVDC corridor. The HVDC tapping station is a possible solution to overcome this issue [6], [7], [8]. These HVDC taps can be designed to be bidirectional, thus they are able to inject or consume power. This concept allows to integrate offshore wind energy without building a whole HVDC link, a key factor in terms of reduction investment. An LCC-HVDC parallel tap based on Voltage Source Converters (VSC) is proposed in [9] for integration of wind power. Nonetheless, it does not allow power reversal in the LCC link while the tapping station is operational. A series tapping station based on a CSC for offshore wind power integration was introduced in [10]. CSCs has been considered for high voltage purposes in several papers: [11] presents a CSC based Static Synchronous Compensator (STATCOM), an HVDC link based on two CSCs is introduced in [12], an hybrid system with one CSC and a LCC is proposed in [13], [14] and several cascaded CSCs in both OWPP side and grid side of the HVDC link are suggested in [15], [16]. Several more applications can be found in [17]. It has also been considered as a full-power converter for wind turbines [18], [19], [20]. CSC is suitable to be in series with LCC-HVDC as they share some features, for instance, DC current flows always in the same direction and voltage can

be bidirectional. CSC technology allows the regulation of active and reactive power independently, it has black-start capability and the required filters are smaller than LCC-HVDC. CSCs require switches with reverse-blocking voltage capability. A diode can be placed in series with the IGBT to achieve this behaviour [21]. Other options are: Reverse-Blocking IGBT (RB-IGBT) with intrinsic diode, Gate Turn-Off thyristor (GTO) and Integrated Gate Commutated Thyristor (IGCT) could also be considered [22],[23].

[Figure 1 about here.]

This paper extends the work presented in [10]. A series tapping CSC for integrating offshore wind energy into an LCC-HVDC link is discussed. A coordinated control of the CSC and the OWPP is designed. A steady-state analysis considering the modulation limit of the CSC is performed for different voltage levels and powers. A Power Reduction Algorithm (PRA) is proposed in order to address system control when the CSC is not able to extract all the power from the OWPP. Three scenarios are simulated to test the behaviour of the system: a DC current reduction in the HVDC link with and without the proposed PRA and a loss of communications between the CSC and the OWPP.

The paper is organized as follows: Section 2 describes the studied system. Section 3 presents the system modelling. Section 4 introduces the operation and control of all power converters. The steady-state analysis based on the modulation limit of the CSC is presented in Section 5. Section 5 also illustrates several considerations on system reliability and proposes a PRA. Dynamic simulations to verify the system control under normal operation with the DC current reduction and under loss of communication are depicted in section 6. Finally, section 7 summarises the conclusions of the work.

2. System description

Fig. 2 shows the LCC-HVDC transmission system and the interconnection of an OWPP by means of a bidirectional CSC connected in series with the HVDC link.

[Figure 2 about here.]

The LCCs are twelve-pulse bridges with their two corresponding transformers (star-star and star-delta). The converter stations include proper tuned AC filters and they are connected to two different AC grids. CSC is a two-level converter made of six switches with reverse blocking voltage capability (IGBT with a diode in series) [21]. Finally, the OWPP is composed of m clusters of n turbines each. The wind turbines are based on full-power converter Permanent Magnet Synchronous Generator (PMSG). System parameters can be found in Table 1 and Table 2.

3. System modelling

3.1. LCC-HVDC transmission system

The modelling of LCC stations is based on the CIGRE benchmark [24]. LCC1 is acting as a rectifier and LCC2 is operating in inverter mode.

3.2. Current Source Converter

The CSC is modelled as a two-level converter. A multilevel topology can also be considered for the real implementation [25]. Modulation is based on [26]. It is directly connected to the AC capacitors of the OWPP as depicted in Fig. 3.

[Figure 3 about here.]

Park's transformation used is:

$$\mathbf{T}(\theta) = \frac{2}{3}\begin{bmatrix} \cos(\theta) & \cos(\theta - \frac{2\pi}{3}) & \cos(\theta + \frac{2\pi}{3}) \\ \sin(\theta) & \sin(\theta - \frac{2\pi}{3}) & \sin(\theta + \frac{2\pi}{3}) \\ \frac{1}{2} & \frac{1}{2} & \frac{1}{2} \end{bmatrix} \tag{1}$$

The plant of the system are the AC capacitors which can be described in the qd reference as (2).

$$\begin{bmatrix} i_{xq} \\ i_{xd} \end{bmatrix} - \begin{bmatrix} i_{mq} \\ i_{md} \end{bmatrix} = \begin{bmatrix} 0 & \omega_e C_{wf} \\ -\omega_e C_{wf} & 0 \end{bmatrix} \begin{bmatrix} v_{cq} \\ v_{cd} \end{bmatrix} + \begin{bmatrix} C_{wf} & 0 \\ 0 & C_{wf} \end{bmatrix} \frac{d}{dt} \begin{bmatrix} v_{cq} \\ v_{cd} \end{bmatrix} \tag{2}$$

where, i_{xqd} is the current modulated by the converter, i_{mqd} is the current coming from the OWPP and v_{cqd} are the components of the capacitor voltage. ω_e is the grid frequency and C_{wf} is the capacitance of the AC capacitors.

3.3. Offshore Wind Power Plant

Only one single wind turbine is modelled and it is assumed that all wind turbines have the same wind speed in order to simplify the analysis. The wind turbine is modelled using the three blade horizontal axis characteristic. It is coupled with a gearless Permanent Magnet Synchronous Generator (PMSG). The machine is connected to a full-rated VSC in *back-to-back* configuration. The behaviour of a whole OWPP is obtained through an aggregate model [27]. Fig. 4 illustrates the model of one wind turbine.

[Figure 4 about here.]

3.3.1. Wind turbine

The wind turbine is modelled according to the power equation [28]:

$$P_t = \frac{1}{2} C_p p A v_{wind}^3 \tag{3}$$

where, C_p is the power coefficient, p is the density of air, A is the swept area of turbine blades and v_{wind} is the wind speed. The turbine is gearless coupled to a PMSG, thus, the transmission equation is [28]:

$$\Gamma_m - \Gamma_e = J_t \frac{d}{dt} \omega_t \tag{4}$$

where, Γ_m and Γ_e is the mechanical and electrical torque, respectively. J_t is the inertia of the wind turbine and the PMSG and ω_t is the rotational speed of the turbine.

3.3.2. Generator side VSC

Both VSCs are modelled using the average model described in [29]. The generator side VSC is connected to the PMSG and the system is modelled using equation (5) [30].

$$\begin{bmatrix} v_{sq} \\ v_{sd} \end{bmatrix} = \begin{bmatrix} r_s & \omega_t p L_s \\ -\omega_t p L_s & r_s \end{bmatrix} \begin{bmatrix} i_{sq} \\ i_{sd} \end{bmatrix} + \begin{bmatrix} L_s & 0 \\ 0 & L_s \end{bmatrix} \frac{d}{dt} \begin{bmatrix} i_{sq} \\ i_{sd} \end{bmatrix} + \lambda_m p \omega_t \begin{bmatrix} 1 \\ 0 \end{bmatrix} \tag{5}$$

where, v_{sq} and v_{sq} are the stator voltages, r_s and L_s are the stator resistance and inductance, respectively. p is the pole pairs of the generator and λ_m is the flux linkage.

The PMSG is based on a round-rotor, therefore, the electrical torque is proportional to q component of stator current (6).

$$\Gamma_e = \frac{3}{2} p \lambda_m i_{sq} \tag{6}$$

3.3.3. Grid side VSC

The grid side VSC is connected to the AC grid of the OWPP. The equation describing the system is [31]:

$$\begin{bmatrix} v_{tq} \\ 0 \end{bmatrix} - \begin{bmatrix} v_{bq} \\ v_{bd} \end{bmatrix} = \begin{bmatrix} r_{wf} & \omega_e L_{wf} \\ -\omega_e L_{wf} & r_{wf} \end{bmatrix} \begin{bmatrix} i_{bq} \\ i_{bd} \end{bmatrix} + \begin{bmatrix} L_{wf} & 0 \\ 0 & L_{wf} \end{bmatrix} \frac{d}{dt} \begin{bmatrix} i_{bq} \\ i_{bd} \end{bmatrix} \tag{7}$$

where, v_t is the voltage before the coupling inductances, v_b is the voltage modulated by the converter. i_b is the current through the converter, L_{wf} is the inductance value and r_{wf} is the parasitic resistance of the coupling inductances. The full-rated converter also includes a Dynamic Breaking Resistor (DBR), modelled as a current source, described by equation (8).

$$I_{dbr} = \frac{E_{btb}}{R_{dbr}} q \tag{8}$$

where, E_{btb} is the DC voltage of the full-rated converter, R_{dbr} is the resistance value of the DBR and q is de modulation factor of the DBR switch.

4. System control design

4.1. LCC-HVDC transmission system

The LCC-HVDC link is operated according to the following strategy: LCC rectifier regulates DC current to the nominal value in normal operation while LCC inverter controls the DC voltage. The V_{dc} reference in the inverter is compared with the measured DC voltage of the link, V_2, and introduced in a PI obtaining the firing angle. The I^*_{dc} reference comes from the Voltage Dependent Current Order Limiter (VDCOL) and it is compared with the measured value and introduced in a PI obtaining the firing angle of the rectifier. The input for the VDCOL is the measured DC voltage of the link, V_1. VDCOL allows to operate the system with low currents when the voltage reference of

the LCC inverter is also reduced. It also diminishes DC current reference if a fault appears on the inverter side. Controllers are tuned to achieve a first order response using the average model presented in [32]. A scheme of the control methodology is depicted in Fig. 5. The VDCOL is depicted in Fig. 6.

[Figure 5 about here.]

[Figure 6 about here.]

4.2. Current Source Converter

The CSC maintains constant AC voltage in the OWPP AC grid and it absorbs the incoming power of the OWPP. For this work, it is assumed that all available wind power will be injected into the LCC link independently of the power demand in the LCC transmission system. The control is designed using an average model of the converter based in three ideal current sources and vector control strategy is applied [10]. The control scheme is based on a voltage loop and is depicted in Fig. 3. The system (2) is decoupled using (9), what leads to (10):

$$\begin{bmatrix} i_{xq} \\ i_{xd} \end{bmatrix} = \begin{bmatrix} \hat{i}_{xq} + i_{mq} + \omega_e C_{wf} v_{cd} \\ \hat{i}_{xd} + i_{md} - \omega_e C_{wf} v_{cq} \end{bmatrix} \tag{9}$$

$$\begin{bmatrix} \hat{i}_{xq} \\ \hat{i}_{xd} \end{bmatrix} = \begin{bmatrix} C_{wf} & 0 \\ 0 & C_{wf} \end{bmatrix} \frac{d}{dt} \begin{bmatrix} v_{cq} \\ v_{cd} \end{bmatrix} \tag{10}$$

where $\hat{i}_{xq}$ and $\hat{i}_{xd}$ are the new decoupled current variables. From equation (10), transfer function for the capacitors can be deduced for both qd components:

$$\frac{V_{cq}(s)}{\hat{I}_{xq}(s)} = \frac{1}{C_{wf}s} \qquad \frac{V_{cd}(s)}{\hat{I}_{xd}(s)} = \frac{1}{C_{wf}s} \tag{11}$$

The transfer functions of the system are two integrators. Applying Internal Model Control (IMC) technique to tune the controllers to achieve a first order response, a proportional controller is obtained. However, any disturbance introduces steady-state error. For this reason, a IMC methodology improved for disturbance rejection is applied [33], obtaining a proportional-integral-derivative (PID) controller.

4.3. Wind turbine

Wind turbine operates following the optimum power curve [28] for low winds. A pitch control and an pitch actuator are included in the system in order to limit power extraction. When the measured electrical power, P_{PMSG}, is exceeding the reference, the pitch control increases the pitch angle to reduce the power extraction and maintain the turbine operating at nominal power, P_{nom}. Pitch control is designed according *gain scheduling* technique [34]. Fig. 7 shows the operation characteristic $P_t - v_{wind}$ of the wind turbine [34].

[Figure 7 about here.]

The control scheme of the wind turbine is depicted in Fig. 8.

[Figure 8 about here.]

4.3.1. Generator side VSC

Control design is based on the average model of the VSC [29]. The generator side uses the classical vector control and it is operating with *maximum torque control* [30]. The electrical torque is proportional to the q component of the stator current (6) and d component of the current is set to 0. It extracts the maximum power of the wind turbine by driving it to the optimal rotational speed, ω_{opt}. The control scheme includes one current loop to regulate q and d components of the stator current. The obtained controllers are two PI designed using IMC methodology [31] in order to achieve a first order response. The control scheme is depicted in Fig. 8.

4.3.2. Grid side VSC

Control design is based on the average model of the VSC [29]. The grid side converter uses the classical vector control with two cascaded control loops [31]: The inner loop controls current qd components independently while the outer loop regulates the DC voltage. Reactive power is kept to 0, controlling i_{bd} to 0. The PI controllers are also tuned with IMC technique [31]. The Dynamic Breaking Resistor (DBR) is in charge of keeping the DC voltage below its maximum value. It is activated according a

proportional control law when the DC voltage of the VSC, E_{btb}, is within two voltage levels: (E_1 and E_2) [35]. The modulation factor of the DBR switch is described as:

$$q = \frac{E_{btb} - E_1}{E_2 - E_1} \tag{12}$$

where, E_{btb} is the measured DC voltage.

[Figure 9 about here.]

The control scheme of the grid side VSC is illustrated in Fig. 9

5. Power reduction algorithm

5.1. Steady-state analysis during DC current reduction

CSCs based on self-commutating devices modulate current waveforms, instead of voltage waveforms. For a given DC current there is a maximum waveform amplitude that the converter is able to synthesize. Equation (13) express the maximum amplitude of one of the phases [21].

$$i_{x-peak} = \sqrt{i_{xq}^2 + i_{xd}^2} = \frac{\sqrt{3}}{2} M I_{dc} \tag{13}$$

where, M is the modulation factor with a maximum value of 1 to work under over modulation [21] and i_{x-peak} is the amplitude of the current waveform. The DC current of the HVDC link varies within a range established by the VDCOL and the power transfer between LCC stations. This fact may limit the injection of wind power in the HVDC transmission system when current is reduced. In order to address DC current reduction and its effects, the following equation system (14) is solved:

$$i_{mq}^2 + i_{md}^2 = \frac{3}{4} I_{dc}^2 - 2 i_{md} \omega_e v_{cq} - \omega_e^2 C_{wf}^2 v_{cq}^2 \tag{14a}$$

$$P = \frac{3}{2} v_{cq} i_{mq} \tag{14b}$$

$$Q = \frac{3}{2} v_{cq} i_{md} \tag{14c}$$

$$Q = -\frac{\omega_e L_{eq} (i_{mq}^2 + i_{md}^2)}{2r^2} \tag{14d}$$

where, P and Q are the active power and reactive power at the AC capacitors. L_{eq} is the equivalent inductance of the OWPP AC grid and r is the relation of the transformer between the CSC and the AC grid. Combining equation (2) with (13), equation (14a) is obtained. Equations (14b) and (14c) are the active and reactive power, respectively, at the AC capacitors. No losses are considered between the VSCs of each wind turbine and the CSC in order to simplify the steady-state analysis. Equation (14d) calculates reactive power considering the equivalent inductance of the OWPP AC grid and the current module after the transformer because it is assumed that each VSC injects no reactive power in the OWPP AC grid. Solving the previous system permits to find the points where the system is operating with the maximum AC current which the converter is able to synthesize. Relations between P, v_{cq} and I_{dc} are depicted in Fig. 10 and Fig. 11 using the results of the previous equation system (14a)-(14d). Fig. 10 shows that the higher the DC current, the higher the maximum power that can be extracted from the OWPP. Fig. 11 shows that AC voltage needs to be higher when there is a DC current reduction in order to inject the same power.

[Figure 10 about here.]

[Figure 11 about here.]

For this study a V_{cq} voltage of 50 kV has been considered. The chosen voltage allows a power transfer of 69% of nominal power at a DC current of 1.1 kA (minimum value of the VDCOL). When the current rises to 1.6 kA, nominal power of OWPP is guaranteed. In case of need of power reduction, during a drop of DC current, an algorithm to address this problem is presented in section 5.3.

5.2. Considerations on system reliability

The addition of the CSC based series tapping station can decrease the reliability of the system if some measures are not taken into account. A solution more independently in terms of operation can be an HVDC point-to-point connection for the OWPP. Nonetheless, it would require an additional main converter and DC cables of several

kilometres, a considerable increase in cost. The main considerations are presented below:

Firstly, the CSC must have bypass switches in order to bypass the converter and allow the operation of the system as a conventional LCC-HVDC link when it is desired.

Secondly, communications between the LCC stations and the CSC are required. For instance, it may be necessary due to market regulation or technical causes that the OWPP modify its power injection. In such situations, both LCC stations should be able to command to the CSC station to initiate or finalize its operation, as well as, changing its power reference.

Finally, the issue raised in Section 5.1 about DC current reduction is addressed using a power reduction algorithm in Section 5.3

5.3. Proposed Power Reduction Algorithm (PRA)

Three different approaches can be considered to address the DC current reduction in the LCC-HVDC link: The first approach is to guarantee that in the worst case (minimum DC current in the HVDC link), the CSC must be able to extract the nominal power of the OWPP. The second approach is introducing a power reduction algorithm in the OWPP to diminish wind power when DC current is low. The third approach is to adapt the VDCOL algorithm to the CSC and OWPP requirements.

The third option is not desirable as the OWPP represents a 10% of the nominal power of the link and the idea is not to modify the control and operation algorithms of the transmission system. The first approach simplifies the control design as it ensures that for any wind power, the CSC is capable of injecting all power into the HVDC link. Nonetheless, it requires high AC voltages in the OWPP that can lead to a cost increase not affordable by the increment in wind power extraction. The second approach permits lower AC voltage but needs an additional power reduction algorithm and communications between the CSC and the wind turbines. For this work, the second approach has been considered and the procedure implemented is as follows.

The first step is saturating the q component of the current of the grid side VSC of each turbine according with maximum value of i_m that the CSC is able to absorb.

From expression (14a) and considering the transformer ratio and the total number of wind turbines in the OWPP, the maximum peak value of current injected by each grid side VSC is:

$$i_{cr} = \sqrt{\frac{1}{r^2 m^2 n^2}\left(\frac{3}{4}I_{dc}^2 - 2\omega_e i_{md} v_{cq} - \omega_e^2 C_{wf}^2 v_{cq}^2\right)} \tag{15}$$

where, i_{cr} is the maximum value of the q component of the current through grid side VSC of each turbine, i_b. r is the transformer ratio, m is the number of wind turbine clusters and n is the number of wind turbines in each cluster. This current limitation is transformed in a power limitation by means of expression (16).

$$P_{cr} = \frac{3}{2} v_{tq} i_{cr} \tag{16}$$

This power limitation is assumed to be shared equally by all wind turbines. Pitch control also receives the new power reference, P_{cr}, and chooses the minimum value between this one and the nominal power of the turbine P_{nom}. The power reference sent to the pitch controller is set to be lower than P_{cr} in order to have a better control of the VSC voltage by the grid side VSC. A value of a 95% of P_{cr} has been set after performing an heuristic analysis. Then, it increases pitch angle to limit power extraction. Pitch control is much slower than current control in the VSC, therefore, the generator side VSC is absorbing wind power but it cannot be injected into the AC grid. This leads to a transient increase of the DC voltage of the back-to-back converter. A DBR is used to eliminate the exceeding power during these few seconds. During loss of communications between the CSC and the wind turbines, the wind turbines set the power reference to the worst possible scenario (the power that the CSC is able to inject for a DC current of 1.1 kA). Fig. 12 shows the control scheme of one wind turbine with the power algorithm implemented.

[Figure 12 about here.]

Several other approaches could also be considered. For instance, current could be saturated in the generator side VSC, which is equivalent to limit the electric torque. Then, the rotor of the PMSG would be accelerated and the pitch control also would increase pitch angle to keep the turbine below nominal power. This strategy avoids

the DBR to be activated and the exceeding energy is used to accelerate the turbine increasing its mechanical stress. A combination of both ideas can also be an option. Nevertheless, they are not considered in this study since mechanical analysis is not performed.

6. Dynamic simulations

The simulations are performed considering switching models for LCCs and CSC, and average models for VSCs. The system parameters used for the simulations are listed in Table 1 and 2. Table 3 shows the control parameters. Section 6.1 and section 6.2 present the simulation results of a DC current reduction in the HVDC link with and without PRA, respectively. Section 6.3 presents the results during a communication loss between the CSC and the OWPP.

[Table 1 about here.]

[Table 2 about here.]

[Table 3 about here.]

6.1. Start-up and DC current reduction without PRA

Fig. 13 depicts the variables of the HVDC link and the CSC station and Fig. 14 shows the variables of one wind turbine. At the initial instant, the CSC is bypassed and LCC1 is acting as a rectifier and LCC2 as an inverter. The voltage of the HVDC link is ramped until its nominal value (Fig. 13a) while the current is regulated by LCC1 according to the VDCOL (Fig. 13b). The system is operating without absorbing power from the OWPP. At instant $t = 3.5$ s the wind farm is energized. Fig. 13d shows how the AC voltage of the AC grid, v_{cq}, is regulated at 50 kV and the DC bus of the full-rated of each wind turbine is raised until the nominal value (Fig. 14e). During this instant the CSC is consuming power, thus, component i_{mq} has a positive value as it can be seen in Fig. 13f. The generator side VSC starts to apply the maximum power extraction algorithm at $t = 4$ s (Fig. 14b), and the OWPP starts to inject power into

the LCC-HVDC link (Fig. 13c). Fig. 13a shows a negative voltage for the CSC since it is injecting power to the HVDC link. It can be seen that V_1 is lower than V_2, as part of the power is provided by the CSC (Fig. 13c). Fig. 14a depicts the wind profile and Fig. 14c the pitch angle of the wind turbine. The power from the generator is shown in Fig. 14d as P_{PMSG} and P_{btb} is the power injected by each full-power converter to the OWPP grid. DC currents inside the full-power converter are illustrated in Fig. 14f. The AC voltage and the AC current in the CSC can be seen in Fig. 13d and Fig. 13g, respectively. Fig. 13g compares the modulated current of phase a, i_{xa}, with the reference signal for modulation, ${i_{xa}}^*$. It can be noticed that ${i_{xa}}^*$ is lower than the modulation limit, M_{lim}. After instant 7 s, the voltage reference of station LCC2 is reduced (Fig. 13a). Fig. 13b depicts how the VDCOL is also diminishing the DC current to 0.55 pu. This current reduction leads to a decrease of the wind power that the CSC is able to inject due to the current modulation. Fig. 13h shows that the reference current, ${i_{xa}}^*$, to extract the power is higher than the modulation limit, M_{lim}. After instant, $t = 10s$, the CSC is not able to control the AC voltage (Fig. 13e).

[Figure 13 about here.]

[Figure 14 about here.]

6.2. Start-up and DC current reduction with PRA

Fig. 15 and Fig. 16 show the simulation results considering the same conditions that in Section 6.1 but with the PRA implemented. Fig. 15 depicts the variables of the HVDC link and the CSC station and Fig. 16 shows the variables of one wind turbine. Before instant $t = 7s$ the system is evolving with no difference compared with Section 6.1. After this instant, Fig. 15b depicts how the VDCOL is diminishing the DC current to approximately 0.55 pu. This current reduction leads to a decrease of the wind power that the CSC is able to inject due to the modulation limit. The power limitation is calculated in the CSC station and sent considering no delays to all the turbines as P_{cr}. Pitch controller increases pitch angle to decrease the extraction of wind power as it can be seen in Fig. 16c. Fig. 16d depicts how P_{cr} decreases and achieves a lower value

than the power extracted by the generator P_{PMSG}. In this case, the power injected by each VSC *back-to-back* to the OWPP grid, P_{btb}, is saturated also according to the DC current reduction (Fig. 16d). This leads to a transient increase of the VSC voltage (Fig. 16e) that activates the DBR during a reduced period of time in order to eliminate the exceeding power. Fig. 16f shows the DC currents in the VSC. I_{btbm} is the current coming from the generator side VSC that has the same value that the current injected into the OWPP AC grid, I_{btbg}, unless during the activation of the DBR. The current through the DBR is depicted as I_{dbr}. In this case, Fig. 15h shows that the reference signal, ${i_{xa}}^*$, reaches the modulation limit, M_{lim}, but it does not increase beyond this limit. As a result, the CSC is able to regulate the AC voltage of the OWPP to the reference level (Fig. 15e).

[Figure 15 about here.]

[Figure 16 about here.]

6.3. Communication loss

Fig. 17 and Fig. 18 show the simulation results for a loss of communication between the CSC station and the wind turbines. Fig. 17 depicts the variables of the HVDC link and the CSC station and Fig. 18 shows the variables of one wind turbine. At instant $t = 2$ s, there is a loss of communications and it are restored at $t = 10$ s. During this scenario the CSC is applying a negative voltage in the HVDC link (Fig. 17a). Fig. 17b shows how the LCC1 is regulating the DC current to the nominal value. A fraction of the power demanded by terminal LCC2 is provided by the CSC as it can be seen in Fig. 17c while it is controlling the AC voltage of the OWPP to a constant value (Fig. 17d). Fig. 17e shows the component q and component d of the current coming from the OWPP. This graphic illustrates a decrease of current due to the loss of communications. Fig. 17f also shows the sinusoidal waveform of the AC voltage at the OWPP. Fig. 18a shows the wind speed in each wind turbine. Graphic 18b depicts the rotational speed of the wind turbine and the optimal speed to extract the maximum power. It can be seen that during the loss of communications the VSC drives the turbine to work below the

optimal speed in order to reduce the power. Pitch angle in Fig. 18c is also increased to reduce power extraction. In Fig. 18d, P_{cr} is presented and is diminished during the communication loss to the minimum value (equivalent to have a DC current of 1100 A). P_{cr} becomes lower than the power of the generator, P_{PMSG}; therefore, the power reduction algorithm is started and increases pitch angle to reduce the power extracted from the wind. The power injected into the AC grid by the VSCs, P_{btb}, is also saturated according to P_{cr}, though, it is set to be a 5% higher in order to have a better control of the DC bus. In Fig. 18e the voltage of the DC bus of each VSC is increasing when P_{PMSG} is higher than P_{cr}. The DC currents of the back-to-back of each wind turbine are presented in Fig. 18f. It can be seen that during the first instants after second $t = 2$ and before $t = 10$ s, P_{PMSG} is much higher than P_{cr}, thus, the DBR is activated to eliminate part of the power due to the raise of VSC DC voltage. The current extracted by the grid side VSC, I_{btbg}, follows the same shape than the one from the generator side VSC, I_{btbm}, however the first one is lower when the DBR is eliminating power.

[Figure 17 about here.]

[Figure 18 about here.]

7. Conclusions

This work conducts the operation and control of a series CSC in order to integrate offshore wind energy into an LCC-HVDC transmission system. The operation and control is addressed during normal operation, DC current reduction and communication loss. An steady-state analysis shows that during DC current reduction in the HVDC link, the capability to inject power into the link is also reduced for a constant voltage in the OWPP AC grid. A power reduction algorithm is proposed to address this scenario. Simulation results during DC current reduction illustrates that the power algorithm reduces the power extraction using pitch control and the grid side VSC injects power according to the maximum current value that the CSC is able to modulate. The DBR is activated to reduce the transient increases in the VSC voltage. Simulation results during communications loss show that the power limitation is set to the minimum value

considering the minimum possible DC current in the HVDC link. The system reduces the power injection using the same power algorithm and increases power extraction again when communications are restored. The simulation results validate the operation and control of the CSC and the proposed power reduction algorithm.

Acknowledgements

This work has been funded by the Spanish Ministry of Economy and Competitiveness under Project ENE2013-47296 and Project ENE2015-67048-C4-1-R. This research was co-financed by the European Regional Development Fund (ERDF).

[1] European Wind Energy Association, "Wind energy scenarios for 2015".

[2] N. B. Negra, J. Todorovic and T. Ackermann, "Loss evaluationof hvac and hvdc trasmission solutions for large offshore wind farms", *Elect. Power Syst. Res., vol. 76*, pp. 916-927, 2006.

[3] R. P. Bahrman and B. K. Johnson, "The ABCs of HVDC Transmission Technologies", *IEEE Power and Energy Mag.*, pp. 32-44, 2007.

[4] R. Adapa, "High Wire Act", *IEEE Power and Energy Mag.*, pp. 18–29, 2012.

[5] European Netweork of Transmission System Operators for Electricity (ENTSOE), "Statistical Factsheet 2014", pp. 1–8, 2015.

[6] M. Aredes,, C. Portela and F. C. Machado, "A 25-MW Soft-Switching HVDC Tap for 500-kV Transmission Lines", *IEEE Trans. Power Del., vol. 19*, pp. 1835–1842, 2004.

[7] M. Bahram, M, Baker, J, Bowles, R. Bunch, J. Lemay, W. Long, J. McConnach, R. Menzies, J. Reeve and M. Szechtman, "Integration of small taps into (existing) HVDC links", *IEEE Trans. Power Del., vol. 10*, pp. 1699–1706, 1995.

[8] M.R. Aghaebrahimi and R.W. Menzies, "Small Power Tapping from HVDC Transmission Systems: A Novel Approach", *IEEE Trans. Power Del., vol. 12*, pp. 1698–1703, 1997.

[9] R. E. Torres-Olguin, M. Molinas and T. Undeland, "Offshore Wind Farm Grid Integration by VSC Technology With LCC-Based HVDC Transmission", *IEEE Trans. on Sust. Energy., vol. 3*, no. 4, pp. 899-907, 2012.

[10] J. Sau-Bassols, A. Egea-Alvarez, E. Prieto-Araujo and O. Gomis-Bellmunt, "Current Source Converter series tapping of a LCC-HVDC transmission system for integration of offshore wind power plants ", *11th IET Int. Conf. on AC and DC Power Transmission*, pp. 1331-1335, 2007.

[11] Y. Ye, M. Kazerani and V. H. Quintana, "Current-Source Converter Based STATCOM: Modeling and Control", *IEEE Trans. Power Del., vol. 20*, pp. 795-800, 2005.

[12] N. Strech, M. Kazerani and R. El Shatshat, "A Current-Sourced Converter-Based HVDC Light Transmission System", *Ind. Electron. IEEE Int. Symp., vol. 3*, pp. 2001-2006, 2006.

[13] R. E. Torres-Olguin, A. Garces, M. Molinas and T. Underland, "Integration of offshore wind farm using a hybrid HVDC transmission composed by PWM current-source converter and line-commutated converter", *Power and Energy Eng. Conf. (APPEEC)*, pp. 1-4, 2012.

[14] R. E. Torres-Olguin, A. Garces, M. Molinas and T. Underland, "Integration of Offshore Wind Farm Using a Hybrid HVDC Transmission Composed by the PWM Current-Source Converter and Line-Commutated Converter", *IEEE Trans. Energy Conv., vol. 28*, no. 1, pp. 125-134, 2013.

[15] M. Popat, B. Wu and N. R. Zargari, "A Novel Decoupled Interconnecting Method for Current-Source Converter-Based Offshore Wind Farms", *IEEE Trans. on Power Electro., vol. 27*, no. 10, pp. 4224-4233, 2012.

[16] M. Popat, B. Wu, F. Liu, and N. R. Zargari, "Coordinated Control of Cascaded Current-Source Converter Based Offshore Wind Farm", *IEEE Trans. on Sust. Energy., vol. 3*, no. 3, pp. 557-565, 2012.

[17] C. Yuan, X. Yang, D. and C. Yue, "Review on Hybrid HVDC Technology for Integration of Offshore Wind Power Plant", *Wind Integration Workshop*, 2013.

[18] J. Dai, D. Xu and B. Wu, "Unified DC-Link Current Control for Low-Voltage Ride-Through in Current-Source-Converter-Based Wind Energy Conversion Systems", *IEEE Trans. on Power Electro., vol. 26*, no. 1, pp. 288-297, 2011.

[19] A. Nikolic and B. Jeftenic, "Current Source Converter Topologies for PMSG Wind Turbine Applications", *14th Int. Power Electro. and Motion Control Conf. (EPE-PEMC)*, pp. 27-32, 2010.

[20] Z. Wang, B. Yuwen, Y. Lang and M. Cheng, "Improvement of Operating Performance for the Wind Farm With a Novel CSC-Type Wind Turbine-SMES Hybrid System", *IEEE Trans. on Power Electro., vol. 28*, no. 2, pp. 693-703, 2013.

[21] C. Liu, D. Xu and L. Jun, "Three-phase current-source buck type PFC converter with reverse-blocking IGBTs", *IEEE Power Electro. Specialists Conf., PESC*, pp. 1331-1335, 2007.

[22] D. Schreiber, "New power semiconductor technology for renewable energy sources application", *SEMIKRON*, 2005.

[23] J. Dai, D. Xu and B. Wu, "A novel control system for current source converter based variable speed PM wind power generators", *IEEE Power Electro. Specialists Conf., PESC*, pp. 1852-1857, 2007.

[24] M. O. Faruque, Y. Zhang and V. Dinavahi, "Detailed Modeling of CIGRE HVDC Benchmark System Using PSCAD/EMTDC and PSB/SIMULINK", *IEEE Trans. on Power Del., vol. 21*, pp.378-387, 2006.

[25] J. Liang, A. Nami, F. Dijkhuizen, P. Tenca, and J. Sastry, "Current source modular multilevel converter for HVDC and FACTS", *15th European Conf. on Power Electro. and Applications (EPE),*, pp. 1-10, 2013.

[26] X. Wang and B. T. Ooi, "Unity PF current-source rectifier based on dynamic trilogic PWM", *IEEE Trans. on Power Electro., vol. 8*, pp.288-294, 1993.

[27] Y. Q. Jin and P. Ju, "Dynamic Equivalent Modeling of FSIG Based Wind Farm According to Slip Coherency", *Int. Conf. on Sustainable Power Generation and Supply, vol. 8*, pp. 1–7, 2009.

[28] T. Ackermann and L. Soder, "Wind Power in Power Systems", *John Wiley & Sons*, 2005.

[29] G. Zhang, Z. Xu and Y. Cai, "An equivalent model for simulating VSC based HVDC", *Transmission and Distribution Conference and Exposition, IEEE/PES, vol. 1*, pp. 20–24, 2001.

[30] G. Michalke, A. D. Hansen and T. Hartkopf, "Control strategy of a variable speed wind turbine with multipole permanent magnet synchronous generator", *European Wind Energy Conf. EWEC*, 2007.

[31] A. Egea-Alvarez, A. Junyent-Ferre and O. Gomis-Bellmunt, "Active and reactive power control of grid connected distributed generation systems", *Modeling and Control of Sustainable Power Systems, Springer*, pp. 47–81, 2012.

[32] Alstom Grid, "HVDC for beginners and beyond", 2010.

[33] M. Shamsuzzoha and M. Lee, "IMC-PID controller design for improved disturbance rejection of time-delayed processes", *Ind. Eng. Chem. Res., vol. 46*, pp. 2077-2091, 2007.

[34] F. D. Bianchi, H. Battista and R. J. Mantz, "Wind Turbine Control Systems", *Springer*, 2007.

[35] A. Egea-Alvarez, "Multiterminal HVDC transmission systems for offshore wind", PhD Thesis, *Universitat Politecnica de Catalunya*, Barcelona, 2014.

List of Figures

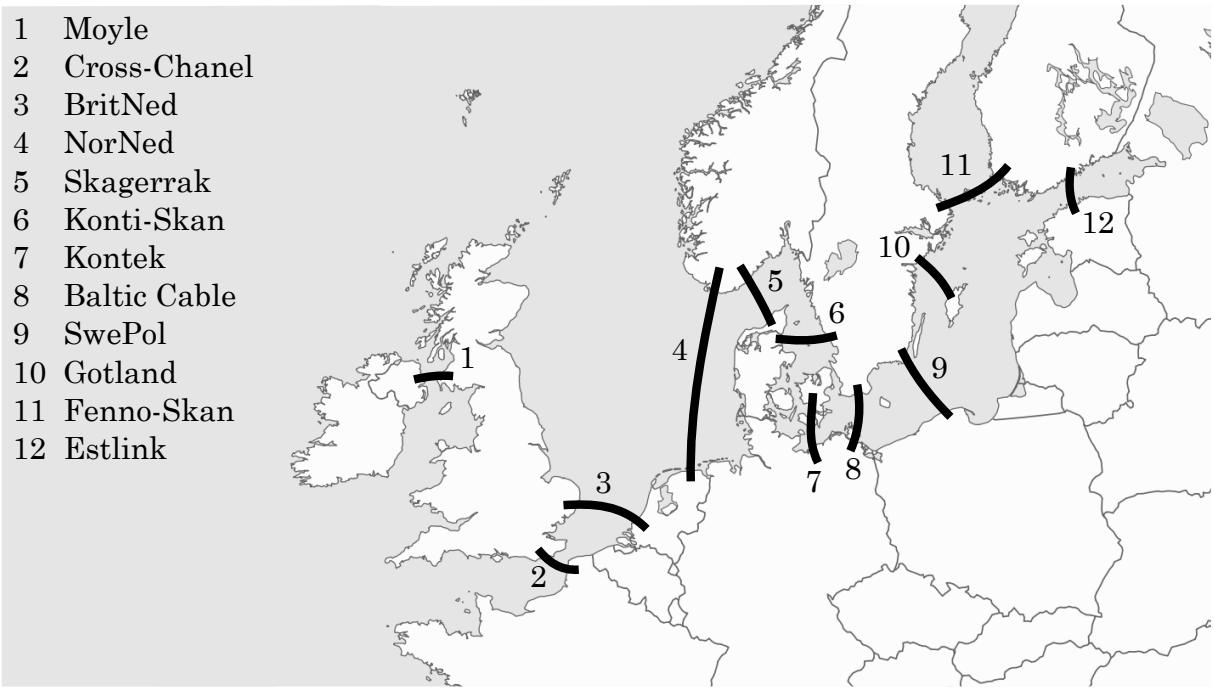

Figure 1: Undersea LCC-HVDC transmission links in Northern Europe

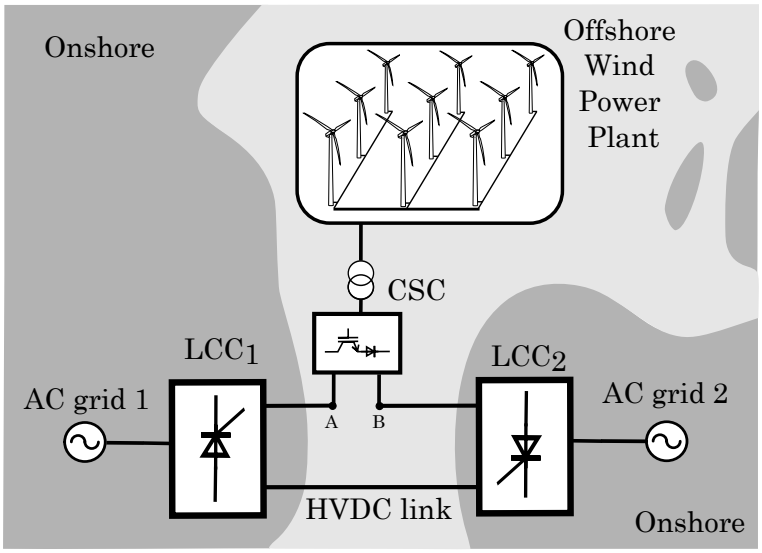

Figure 2: System scheme

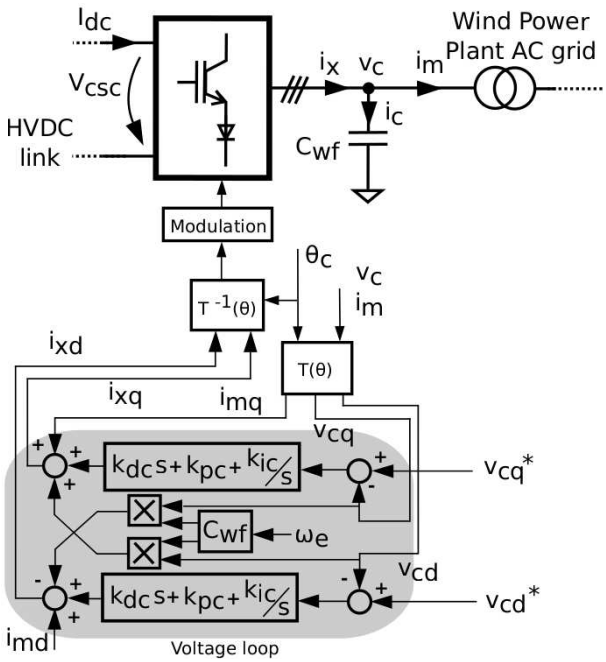

Figure 3: CSC control scheme

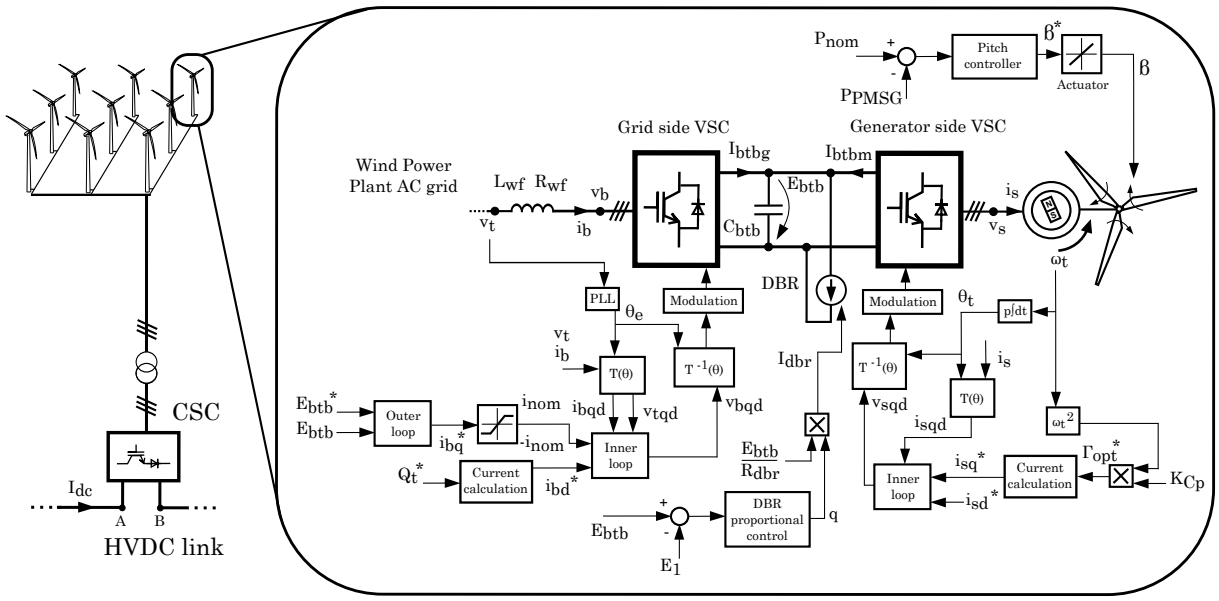

Figure 4: Wind turbine control scheme

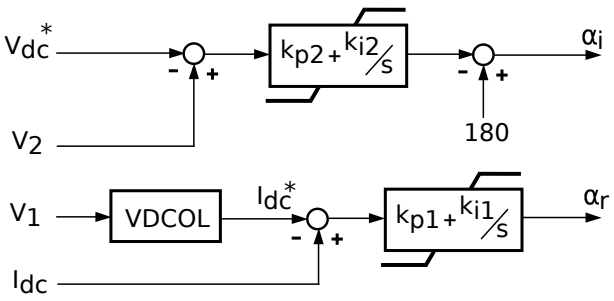

Figure 5: LCC transmission system control scheme

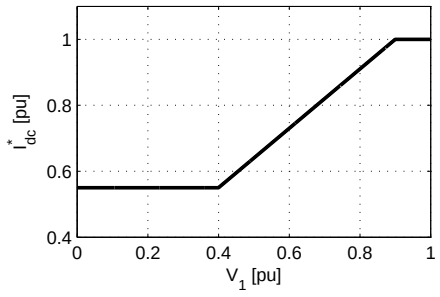

Figure 6: VDCOL law

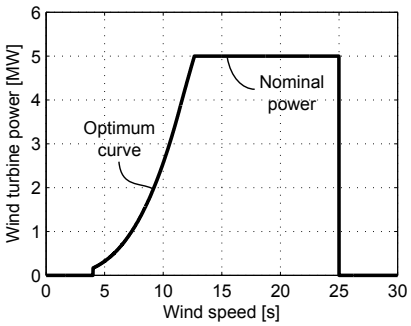

Figure 7: Wind turbine characteristic

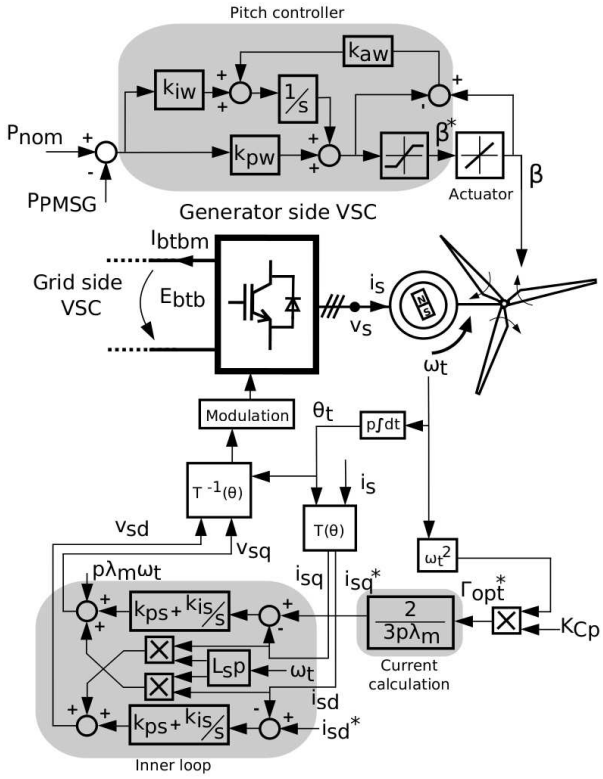

Figure 8: Wind turbine and generator side VSC control scheme

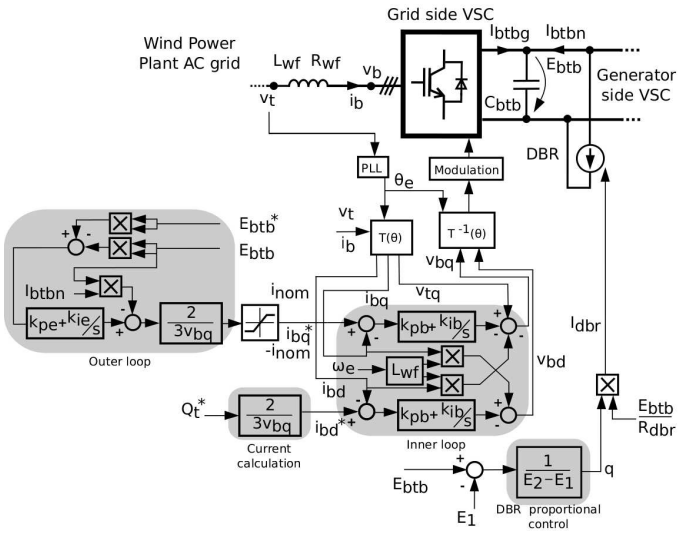

Figure 9: Grid side VSC control scheme

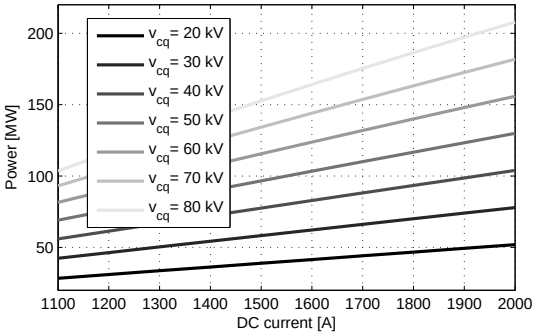

Figure 10: Relation $P - I_{dc}$ for different voltages v_{cq}

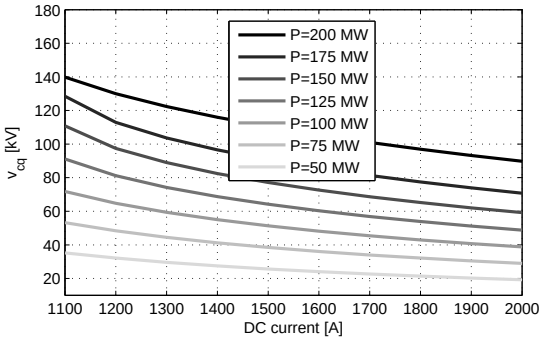

Figure 11: Relation $v_{cq} - I_{dc}$ for different active powers P

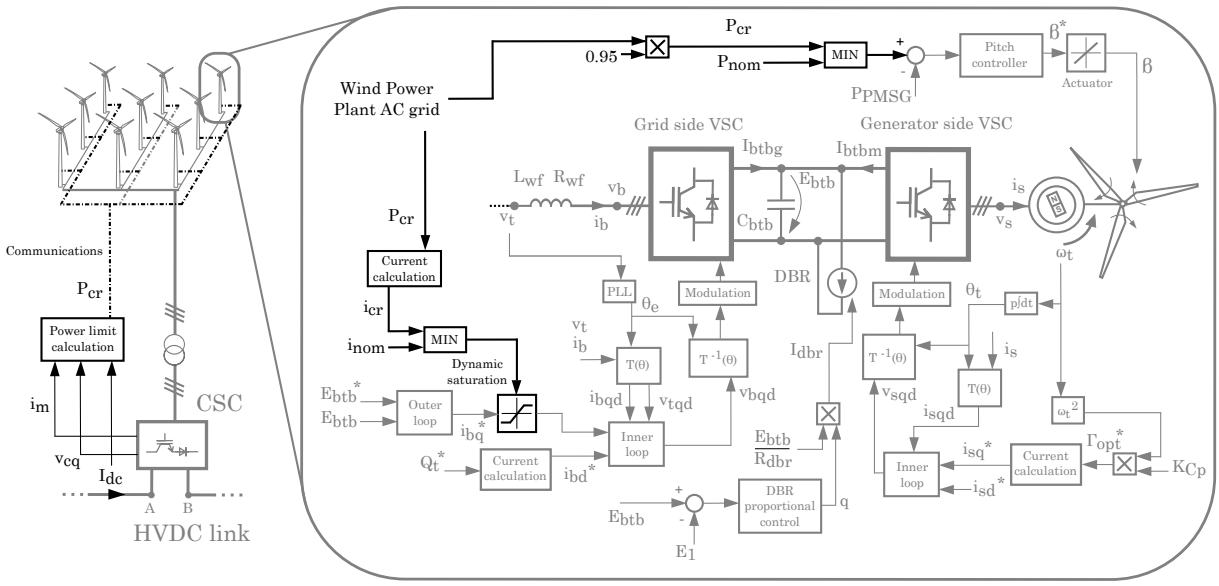

Figure 12: Wind turbine control scheme with the proposed power reduction algorithm

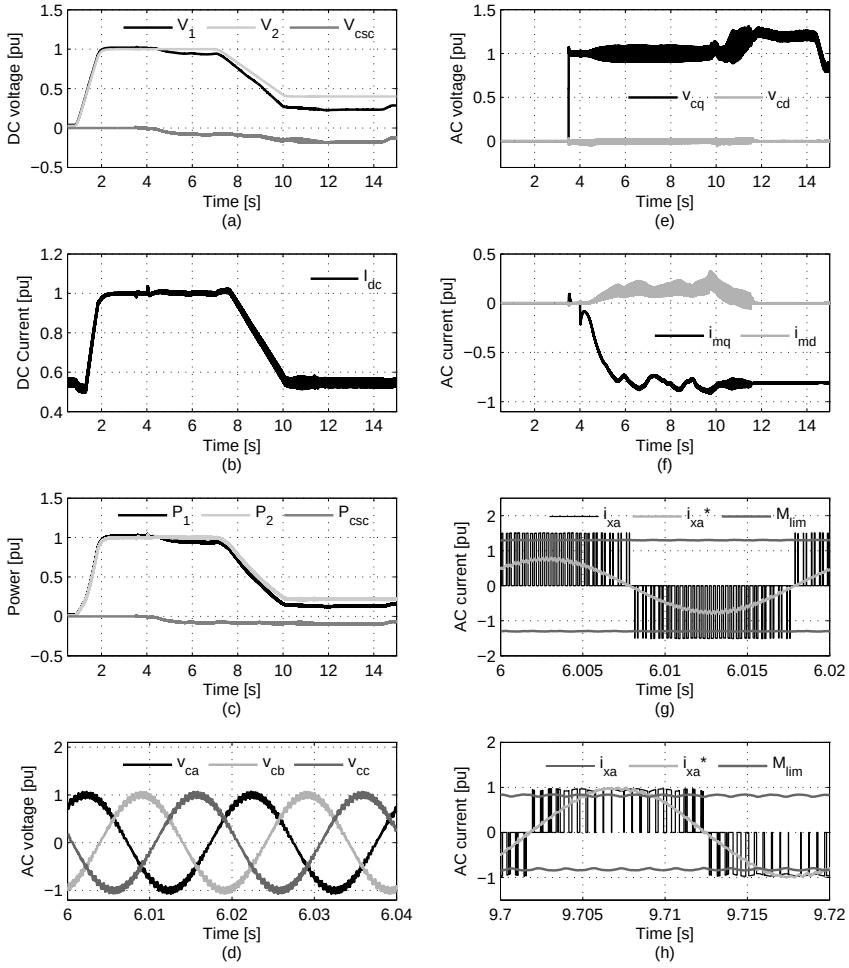

Figure 13: Simulation results for CSC start-up and DC current reduction without PRA: LCC-HVDC and CSC variables

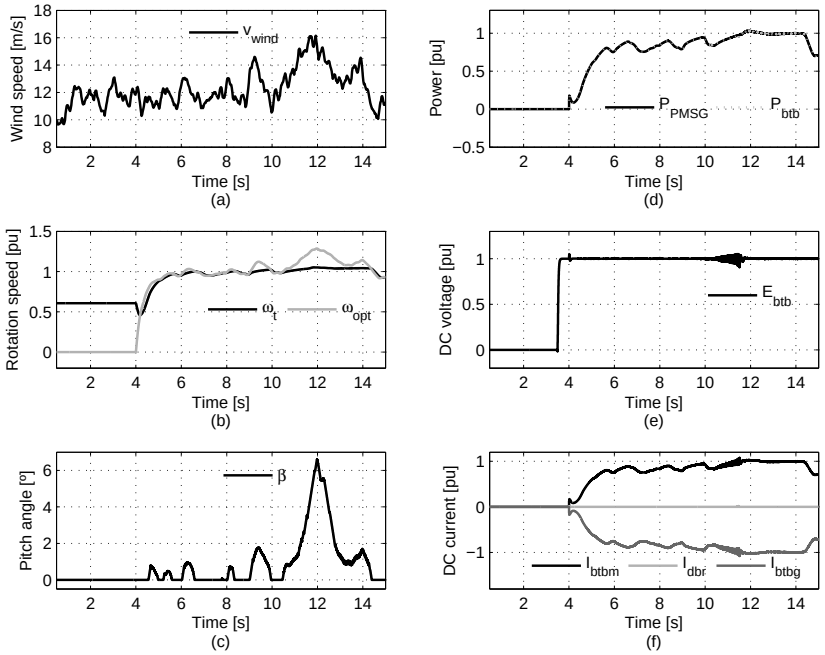

Figure 14: Simulation results for CSC start-up and DC current reduction without PRA: Wind turbine and VSCs variables

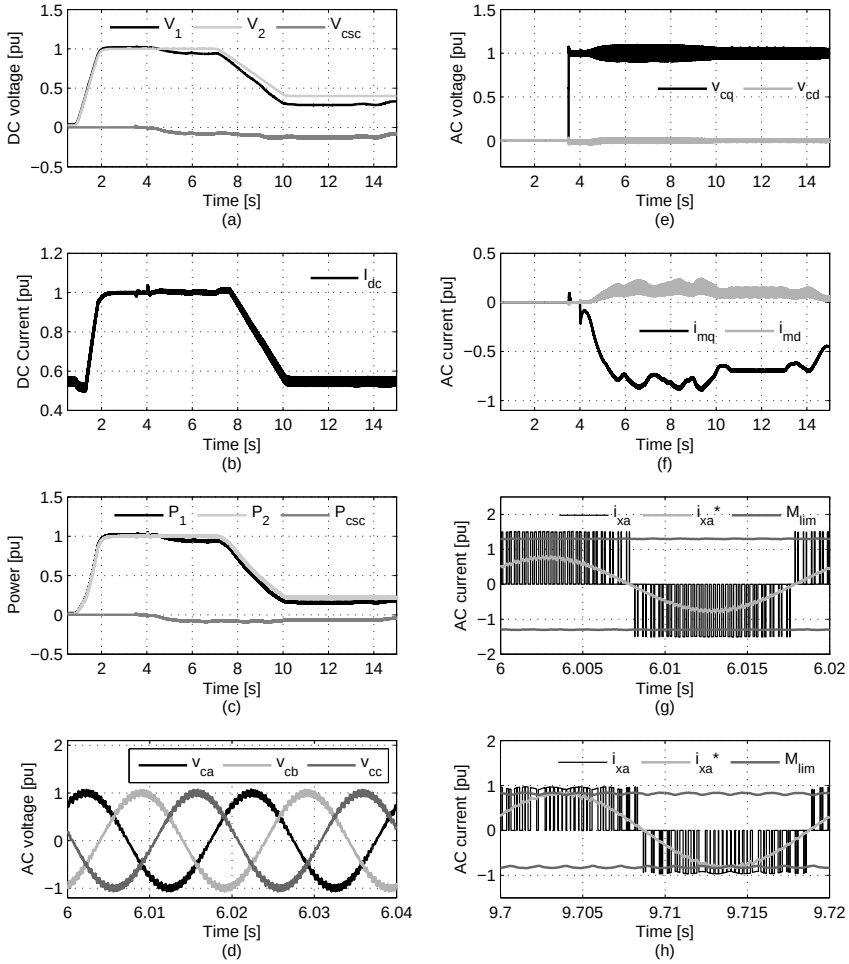

Figure 15: Simulation results for CSC start-up and DC current reduction with PRA: LCC-HVDC and CSC variables

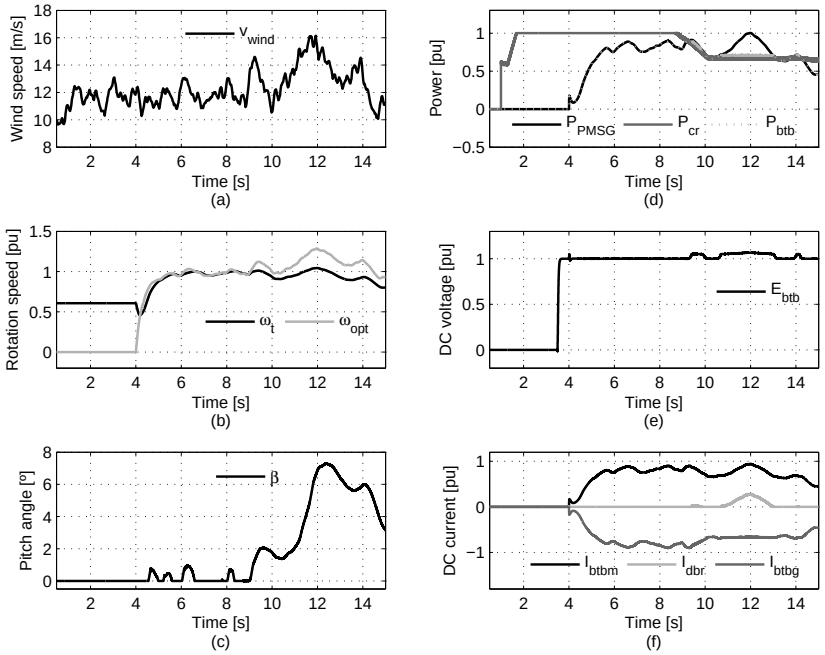

Figure 16: Simulation results for CSC start-up and DC current reduction with PRA: Wind turbine and VSCs variables

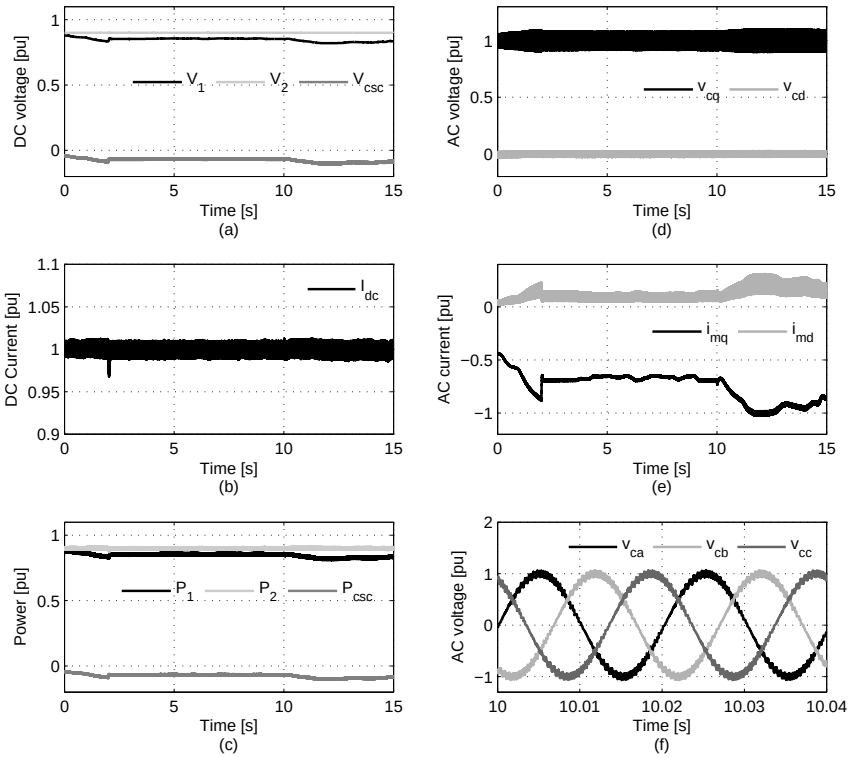

Figure 17: Simulation results during loss of communication: LCC-HVDC and CSC variables

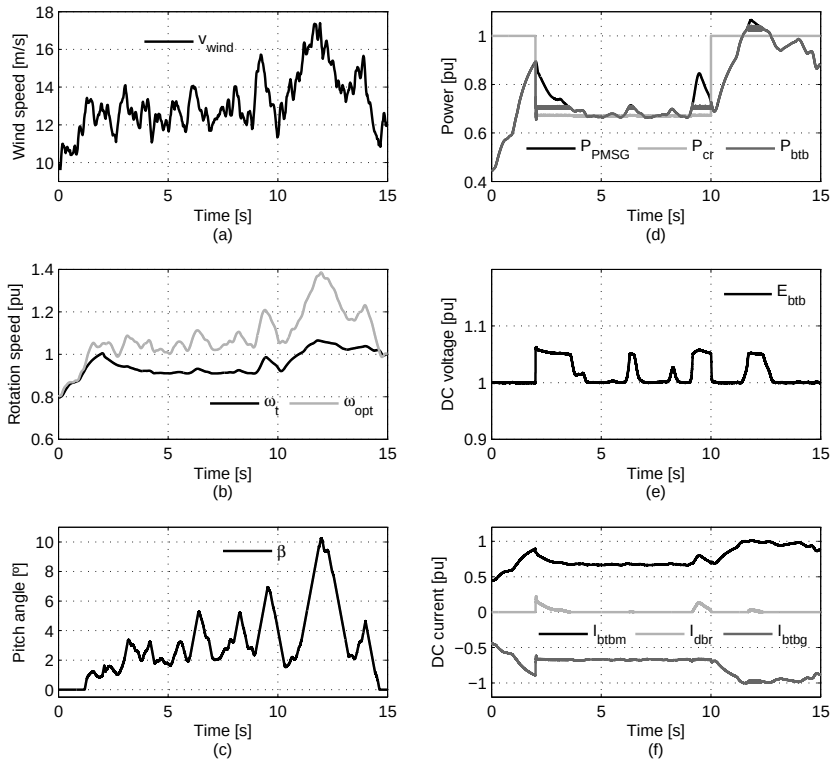

Figure 18: Simulation results during loss of communication: Wind turbine and VSCs variables

List of Tables

Table 1: LCC-HVDC parameters

LCC-HVDC transmission system			
Nominal power	P_{HVDC}	1000	[MW]
Nominal voltage	V_{HVDC}	500	[kV]
Nominal current	I_{HVDC}	2	[kA]
Cable length	l	200	[km]
Cable resistance	r_{cable}	0.25	[Ω/km]
Cable inductance	l_{cable}	5.9	[mH/km]
Cable capacitance	c_{cable}	0.13	[μF/km]
AC grid 1 voltage	V_{ac1}	345	[kV]
AC grid 2 voltage	V_{ac2}	230	[kV]
AC grid 1 inductance	L_{ac1}	0	[mH]
AC grid 2 inductance	L_{ac2}	16.5	[mH]
AC grid 1 frequency	f_{ac1}	50	[Hz]
AC grid 2 frequency	f_{ac2}	50	[Hz]

Table 2: CSC and OWPP parameters

Current Source Converter			
Nominal AC voltage	V_c	61.2	[kV]
AC capacitor	C_{wf}	20.6	[μF]
HVDC transformer leakage inductance	L_{tr2}	8.14	[mH]
HVDC transformer resistance	R_{tr2}	0.256	[Ω]
HVDC transformer relation	r	0.8	-
Switching frequency	f_s	1000	[Hz]
Equivalent inductance of the OWPP AC grid	L_{eq}	12.8	[mH]
Offshore Wind Power Plant			
Number of wind turbines per cluster	n	4	-
Number of wind turbine clusters	m	5	-
Full-rated VSC voltage	E_{btb}	7	[kV]
VSC transformer leakage inductance	L_{tr1}	41.59	[mH]
VSC transformer leakage inductance resistance	R_{tr1}	1.31	[Ω]
VSC capacitance	C_{btb}	1	[μF]
VSC coupling inductance	L_{btb}	103	[mH]
VSC coupling inductance resistance	R_{btb}	1.63	[Ω]
DBR high voltage level	E_2	1.1	[pu]
DBR low voltage level	E_1	1.05	[pu]
DBR value	R_{dbr}	11.86	[Ω]
Wind turbine power	P_{nom}	5	[MW]
Wind turbine rotational speed	ω_{nom}	15.7	[rpm]
Wind turbine inertia	J_t	43.8	[Mgm^2]
Wind turbine swept area	A	10,568	[m^2]
Cut-in speed	v_{in}	4.5	[m/s]
Cut-off speed	v_{off}	25	[m/s]
Pitch actuator speed	v_{pitch}	$\pm$8	[/s]
Pairs of poles	p	100	-
Stator inductance	L_s	8.4	[mH]
Stator resistance	r_s	0.08	[Ω]

Table 3: Control parameters

LCC			
k_{p1}	0.0315	k_{pb}	5.1995
k_{i1}	0.9053	k_{ib}	81.5
k_{p2}	1.7e-7	k_{pe}	0.0439
k_{i2}	0.0010	k_{ie}	1.0622
CSC		Generator VSC	
k_{pc}	0.0091	k_{ps}	1.676
k_{ic}	1.0965	k_{is}	16
k_{dc}	7.5e-7	k_{pw}	8.39e-05
Grid VSC		k_{iw}	1.08e-04
		k_{aw}	43.6186